

Low pH and Anionic Lipid Dependent Fusion of Uukuniemi Phlebovirus to Liposomes

David Bitto¹, Steinar Halldorsson¹, Alessandro Caputo^{1,2}, and Juha T. Huiskonen^{1,#}

¹Division of Structural Biology, Wellcome Trust Centre for Human Genetics, Roosevelt Drive, University of Oxford, OX3 7BN Oxford, UK

²Current address: Department of Biochemistry, South Parks Road, University of Oxford, OX1 3QU Oxford, UK

Running title: Fusion Mechanism of Uukuniemi Phlebovirus

To whom correspondence should be addressed: Juha T. Huiskonen; Oxford Particle Imaging Centre, Division of Structural Biology, Wellcome Trust Centre for Human Genetics, Roosevelt Drive, University of Oxford, OX3 7BN Oxford, UK; Telephone: +44 (0)1865 287844; Email: juha@strubi.ox.ac.uk;

Keywords: Virus entry, virus structure, membrane, membrane fusion, electron tomography, bis(monoacylglycerol)phosphate, bunyavirus, phlebovirus

ABSTRACT

Many phleboviruses (family *Bunyaviridae*) are emerging, medically important viruses. These viruses enter target cells by endocytosis and low pH dependent membrane fusion in late endosomes. However, the necessary and sufficient factors for fusion have not been fully characterized. We have studied the minimal fusion requirements of a prototypic phlebovirus, Uukuniemi virus, in an *in vitro* virus–liposome assay. We show that efficient lipid mixing between viral and liposome membranes requires close-to-physiological temperatures and phospholipids with negatively charged headgroups, such as the late endosomal phospholipid bis(monoacylglycerol)phosphate (BMP). We further demonstrate that BMP increases Uukuniemi virus fusion beyond the lipid mixing stage. By using electron cryo-tomography of viral particles in presence or in absence of liposomes, we observed that the conformation of phlebovirus glycoprotein capsomers changes from the native conformation towards a more elongated conformation at fusion-permissive pH. Our results suggest a rationale for phlebovirus entry in late endosomes.

harbor a negative-sense, segmented single-stranded RNA genome (1). Members of the genus *Hantavirus* are transmitted to humans from rodents, whereas members of the genera *Phlebovirus*, *Orthobunyavirus*, and *Nairovirus* are zoonotic arboviruses; they are transmitted to humans from their animal reservoirs *via* arthropod vectors, such as mosquitoes or ticks (2). Tospoviruses, which infect plants, are also transmitted by arthropods, such as thrips (3).

Notable examples of highly pathogenic bunyaviruses include Crimean–Congo hemorrhagic fever virus (*Nairovirus*) (4) and members of the *Phlebovirus* genus, such as Rift Valley fever virus (5), and severe fever with thrombocytopenia syndrome virus (6, 7). The former, as well as the recently emerged Schmallenberg virus (*Orthobunyavirus*), have been associated with significant loss of livestock (5, 8). Despite the medical and agricultural relevance of bunyaviruses, we are only starting to unravel how they enter their host cells. Understanding virus entry in detail can be of paramount importance in designing anti-viral therapies, none of which are currently available to specifically treat bunyaviral diseases.

Many enveloped viruses enter the cell by endocytosis, as originally demonstrated for Semliki Forest virus (SFV¹; *Alphavirus*,

The family *Bunyaviridae* comprises the largest group of viruses and is divided into five genera (*Phlebovirus*, *Orthobunyavirus*, *Nairovirus*, *Hantavirus*, and *Tospovirus*). Members of this family are enveloped and

¹ The abbreviations used are: SFV, Semliki Forest virus; DC-SIGN, dendritic cell-specific intercellular adhesion molecule-3-grabbing non-

Togaviridae) in 1980 (9, 10). Within the family *Bunyaviridae*, this process is best understood for phleboviruses. A C-type lectin, dendritic cell-specific intercellular adhesion molecule-3-grabbing non-integrin (DC-SIGN) has been shown to mediate entry of phleboviruses into a number of cell lines, including dendritic cells (11). Endocytic routes of phlebovirus infection have been shown to be largely clathrin-independent (12) and caveolin-dependent (13). After endocytosis, phleboviruses are transported to early endosomes (EEs) where they detach from their receptor and continue to late endosomes (LEs) (11), from which viral penetration into the cytosol is thought to take place (12), presumably *via* membrane fusion catalyzed by the viral fusion glycoprotein G_C. The recently solved crystal structure of Rift Valley fever virus (RVFV) G_C revealed a classical class II fusion protein architecture (14), observed earlier in alphaviruses (15) and flaviviruses (16). G_C, together with the glycoprotein G_N, forms laterally connected, ring-shaped assemblies filling the virion surface (17, 18). Structural similarities in the fusion proteins suggests that the membrane fusion mechanism of phleboviruses may be similar to that of other late penetrating viruses harboring class II fusion proteins, such as dengue virus (*Flavivirus*, *Flaviviridae*) (19, 20). However, the phlebovirus fusion mechanism has remained elusive.

We used fluorescence spectroscopy and electron cryo-tomography to study the fusion mechanism of the prototypic phlebovirus,

integrin; EE, early endosome; LE, late endosome; RVFV (Rift Valley fever virus); UUKV, Uukuniemi virus; BMP, bis(monoacylglycerol)phosphate; BHK, baby hamster kidney; GMEM, Glasgow minimal essential medium, SPM, sphingomyelin; FFU, focus-forming unit; PFU, plaque-forming unit; DOPC, 1,2-dioleoyl-sn-glycero-3-phosphocholine; DOPE, 1,2-dioleoyl sn-glycero-3-phosphoethanolamine; Chol, cholesterol; DOPG, 1,2-dioleoyl-sn-glycero-3-phospho-(1'-rac-glycerol); DOPS, 1,2-dioleoyl-sn-glycero-3-phospho-L-serine; PA, phosphatidic acid; PC-pyr, 1-hexadecanoyl-2-(1-pyrenedecanoyl)-sn-glycero-3-phosphocholine; SRB, sulforhodamine B

Uukuniemi virus (UUKV), in a virus–liposome model system. The types of phospholipid species, in addition to pH and temperature, affected membrane fusion. The presence of the late endosomal phospholipid bis(monoacylglycerol)phosphate (BMP) (21) in the liposomes facilitated viral fusion below pH 5.6 and at physiological temperatures. Electron cryo-tomography of virions and virus–liposome complexes provided direct visualization of different stages of fusion, ranging from the pre-fusion state of the viral glycoprotein capsomers to a more extended conformation mediating binding to the target membrane and putative fusion of the two membranes. Taken together, our data provide a rationale for phlebovirus fusion in late endosomes (12), which may not only be facilitated by late endosomal pH, but possibly also by the compartment specific phospholipid BMP.

EXPERIMENTAL PROCEDURES

Cells and viruses—Baby hamster kidney (BHK)-21 cells were provided by Anna Överby (Umeå, Sweden) and grown in Glasgow minimal essential medium (GMEM; Life Technologies, Thermo Fisher Scientific, Waltham, MA), 5% FBS (PAA labs, USA), 10% tryptose phosphate broth (Sigma-Aldrich, St. Louis, MO) and 20 mM HEPES (Life Technologies, Thermo Fisher Scientific, Waltham, MA) at 37 °C in presence of 5% CO₂. UUKV was produced in BHK-21 cells and purified as previously described (12). Briefly, viral supernatants were cleared from cell debris by low speed centrifugation, and the virus particles concentrated by ultracentrifugation of the clarified supernatant through a 20% sucrose cushion at 25,000 rpm (SW32 rotor; Beckman Coulter, Pasadena, CA). Viral pellets were allowed to dissolve overnight in neutral buffer at 4°C and purified over a linear sucrose gradient. For electron cryo-tomography of virus–liposome fusion complexes, sucrose gradient purified UUKV was diluted 10-fold in sucrose-free neutral pH buffer to reduce sucrose concentration, and pelleted again at 4°C for 1 h at 35,000 rpm (TLS-55 rotor; Beckman Coulter, Pasadena, CA). The virus pellet was resuspended in a small remainder of supernatant. For electron cryo-tomography of isolated virions, pelleting of the virus was avoided.

Instead, clarified supernatants were concentrated using centrifugation at 3,000×g in an ultrafiltration device with a 30-kDa cutoff (Vivaspin15R; Sartorius AG, Göttingen, Germany), followed by purification over a linear gradient (8–50% w/v Nycodenz; Progen Biotechnik, Heidelberg, Germany).

Metabolic labeling of UUKV with 1-pyrenehexadecanoic acid (Life Technologies) was performed similarly as described for other viruses (22–24). Briefly, cells were incubated for 48 h in 15 µg/mL 1-pyrenehexadecanoic acid in growth media prior to infection. Cells had to be of low passage number to minimize the cytopathic effect caused by the fluorescent probe. The probe was washed away with serum-free media and cells were infected as described above, in absence of the fluorescent probe. Pyrene-labeled UUKV was concentrated by pelleting and subsequently purified over a sucrose gradient by ultracentrifugation, as indicated above. Virus specific infectivity was estimated by focus-forming unit (FFU) titration (12) and non-reducing SDS-PAGE of virus preparations, using a bovine serum albumin (Thermo Fisher Scientific) standard.

SFV production and pyrene labeling was done essentially as described here for UUKV. Virus production time was 20–24 hours, no sucrose cushion was used in ultracentrifugation and a standard plaque-forming unit (PFU) assay using crystal violet stain (Sigma-Aldrich) was used to determine virus infectivity. As an alternative way to quantify relative concentrations of pyrene-labeled virus stocks, fluorescence emission levels were assessed in presence or absence of 0.2% Triton X-100 by recording emission spectra using a spectrophotometer (Cary Eclipse; Agilent Technologies, Santa Clara, CA). Filters used were 250–395 nm for excitation and 360–1100 nm for emission, using slit-widths of either 5 or 10 nm.

Lipids and liposomes—1,2-dioleoyl-sn-glycero-3-phosphocholine (DOPC), 1,2-dioleoyl-sn-glycero-3-phosphoethanolamine (DOPE), bis(monooleoylglycero)-phosphate (S,R isomer; BMP), cholesterol (ovine wool, >98%), sphingomyelin (brain, porcine), 1,2-dioleoyl-sn-glycero-3-phospho-(1'-rac-glycerol) (DOPG), 1,2-dioleoyl-sn-glycero-3-phospho-L-

serine (DOPS), and L-α-phosphatidic acid (PA; egg, chicken) were purchased from Instruchemie BV (Delfzijl, Netherlands) and 1-hexadecanoyl-2-(1-pyrene-decanoyl)-sn-glycero-3-phosphocholine (PC-pyr) was purchased from Thermo Fisher Scientific (Waltham, MA). All lipids were dissolved in chloroform, except PC-pyr, which was dissolved in ethanol. Dissolved lipids were mixed together in the required molar proportions (Table 1) and the solvent was evaporated in an argon stream. The dried lipids were hydrated to a final concentration of 2 mM total lipid, using 6 mM succinate, 22 mM phosphate, 22 mM glycine (SPG buffer) pH 7.5 including 100 mM NaCl (SPG50N100), by vortexing and thoroughly pipetting up and down. Liposomes containing 1-hexadecanoyl-2-(1-pyrenedecanoyl)-sn-glycero-3-phosphocholine were assessed for pyrene fluorescence by fluorometry, as described above for pyrene-labeled virions. For content mixing assays, liposomes were resuspended in SPG buffer including 75 mM NaCl and 50 mM sulforhodamine B (SRB; Life Technologies). For production of SRB-containing liposomes, lipid hydration was done by shaking the lipids in buffer for 45–60 min at room temperature, followed by thorough resuspension, and performing ten freeze-thaw cycles, alternating between dry ice and 37°C. Liposomes were prepared by extruding hydrated lipids 21 times through polycarbonate membranes (Whatman; GE Healthcare Life Sciences, Buckinghamshire, UK) of 100 nm pore size at room temperature, using a mini-extruder (Avanti Polar Lipids, Alabaster, AL). Lipid mixtures containing sphingomyelin were extruded at 37°C to account for elevated transition temperatures. Excess dye in SRB-labeled liposomes was removed by passing the preparation through a PD Miditrap G-25 column (GE Healthcare Life Sciences, Buckinghamshire, UK). The first ten drops containing the liposomes were collected. Liposome size homogeneity within samples was confirmed by dynamic light scattering.

Lipid mixing assays—Lipid mixing assays were done similarly as previously described for other pyrene-labeled viruses (22–25). UUKV-pyr ($2.4\text{--}6.9 \times 10^7$ FFU) or SFV-pyr ($1.2\text{--}10 \times 10^8$ PFU) at similar excited dimer fluorescence levels were mixed with an excess

of unlabeled liposomes (100 μ L of 2 mM input lipid, assuming insignificant loss of lipids during rehydration) in SPG buffer and 100 mM NaCl (SPG50N100) to a final volume of 1 mL, leading to a maximal sucrose concentration of ~1.2% w/v (assuming a maximum sucrose concentration of 40% in viral stocks) and a total lipid concentration of 200 μ M. Mixtures were pre-incubated at 37°C for 10 min in a quartz cuvette (Hellma Analytics, Müllheim, Germany), after which a pre-titrated amount of 1 M HCl was added to reach the intended low pH. Pyrene excimer fluorescence was measured at 37°C for up to 10 minutes after acidification. Lipid mixing at lower temperatures, as well as in presence of pyrene-labeled liposomes, was performed in the same way. Final pH was verified using a pH microelectrode (Mettler Toledo, Zurich, Switzerland). Total pyrene excimer dilution was induced by addition of a final concentration of 0.2% w/v Triton X-100 (Sigma-Aldrich, St. Louis, MO). Measurements were done using a spectrophotometer (Cary Eclipse; Agilent Technologies, Santa Clara, CA) at 345 nm excitation and 475 nm emission wavelengths with 10-nm slit width. Filters used were 250–395 nm for excitation and 430–1100 nm for emission. To calculate lipid mixing indices, the pyrene excimer fluorescence emission decrease was scaled between an average intensity at neutral pH (defined as 0% lipid mixing), shortly before acidification, and an average after the addition of Triton X-100 (defined as 100% lipid mixing).

Content release assays—In content release assays, SRB-labelled liposomes, equivalent to a total de-quenched fluorescence of 600 to 800 arbitrary units (using 700V photomultiplier voltage), were mixed with UUKV-pyr. The virions were present in similar amounts as used in lipid mixing assays above, but the liposomes were not assumed to be in excess anymore. This experimental setup was chosen as to allow simultaneous detection of both UUKV-pyr (excitation: 345 nm, emission: 475 nm, 5 nm slit width) and SRB-labelled liposomes (excitation: 565, emission: 586 nm, 5-nm slit width). Excitation filter 335–620 nm and emission filter 430–1100 nm were used. The acidification, complete de-quenching and quantification were done essentially as described

above for the lipid mixing assay. To calculate the content release index, the SRB emission was scaled between emission at neutral pH (defined as 0% content release) and emission in presence of 0.2% Triton X-100 (defined as 100% content release).

Cell-cell fusion assays—Cell-cell fusion mediated by UUKV or SFV particles at the cell surface was performed similarly as described earlier (12, 20), with the following modifications. Briefly, BHK-21 cells were washed once in serum-free binding medium (serum-free BHK-21 growth media in presence of 0.2% w/v cell culture grade BSA; Life Technologies) and then incubated for 5 min in presence of 5 μ M BMP at 4°C. After removal of excess BMP, UUKV (m.o.i ~100) or SFV (m.o.i ~70) was added in serum-free binding medium and allowed to bind to cells for 60 min at 4°C. To induce fusion, virus-cell mixtures were treated with binding medium supplemented with 30 mM citrate (final pH 5.0) for 5 min at 37°C. This was followed by a 30-min incubation at 37°C in normal binding medium to facilitate full syncytia formation. In some control experiments, BMP was added to binding medium only at this stage. After fixation in 4% (w/v) formaldehyde in PBS, cell nuclei were stained with Hoechst (8 μ g/ml; Life Technologies, Thermo Fisher Scientific) and membranes with Cell Mask Orange (2 μ g/ml; Life Technologies, Thermo Fischer Scientific) and imaged in PBS. Fluorescence microscopy was performed at room temperature with a Zeiss Observer Z1 spinning disk confocal microscope and a Zeiss 40 \times C-Apochromat NA 1.2 water-immersion objective. Images were acquired from three different experimental replicates for each condition using the Zeiss ZEN Blue software and fusion indices *F* were calculated as previously described (12), using the following formula: $F = [1 - (C/N)]$, where *C* indicates the number of cells and *N* the number of nuclei per field of view (a total of 31–46 fields of view per condition).

Electron cryomicroscopy and tomography—An aliquot (3–4 μ L) of purified virions or virus-liposome complexes was pipetted onto a glow-discharged holey carbon grid (C-flat; Protochips, Raleigh, NC) and 1 μ L of BSA-coated 10 nm gold beads (Aurion;

Wageningen, The Netherlands), used as fiducial markers, was added. For electron cryo-tomography of isolated virions, the grids were washed against pH 7.5 buffer to remove residual Nycodenz (26). For virus–liposome complexes, unlabelled, low sucrose-containing UUKV (~0.1 μ M glycoprotein end concentration) was first mixed with an equal volume of BMP-liposomes at 1 mM end concentration and incubated at 37 °C for 10 minutes to allow possible binding. The grids were washed against 2 mL SPG50N100 adjusted to pH 5.0 or pH 7.5 (control) at 37°C for 20 seconds. Each grid was blotted in a humidified chamber (~70–80% relative humidity) manually from the side opposite of the sample with filter paper to remove excess sample, followed by immediate vitrification in liquid ethane–propane using a vitrification apparatus (CP3; Gatan, Pleasanton, CA). Single-axis tomographic tilt series were collected at 3° increments from –60° to 60° using SerialEM (27) and an electron microscope operated at 300 kV (Tecnai F30 ‘Polara’; FEI, Hillsboro, OR) in low dose mode. Inelastically scattered electrons were filtered in zero-energy-loss mode using an energy filter (Quantum; Gatan, Pleasanton, CA) and 20-eV slit width. Images were acquired at 61,000 \times nominal magnification, corresponding to a calibrated pixel size of 0.31 nm. Defocus values of –6 μ m and –3 μ m were used to image the virus–liposome complexes and virions, respectively. The total electron dose was 100 electrons/ \AA^2 per tilt series. Images were down-sampled to 0.62 nm/pixel prior to reconstruction, and the IMOD package (28) was used to calculate 3D tomograms. Prior to visualization and further processing, the tomograms were low-pass filtered to remove spatial frequencies higher than the first zero in the contrast transfer function of the microscope (1/3.5 nm for tomograms taken at –6 μ m underfocus; 1/2.5 nm for tomograms taken at –3 μ m defocus).

Subtomogram averaging—To solve the structure of the UUKV glycoprotein hexamer, we extracted 96 virions from 9 tomograms for further processing in Jsubtomo (www.opic.ox.ac.uk/jsubtomo) (29, 30) following a gold-standard refinement protocol established earlier (31). Briefly, we first manually picked 54 glycoprotein capsomers

from virion volumes and generated two independent template structures. These templates were used to detect and align all the capsomers in the virions for averaging. A frequency band between 1/3.5–1/18 nm was used in the final round of refinement. Capsomers with the highest cross-correlation and no overlaps to adjacent capsomers (3,008 capsomers) were included in the final average. In the average, the structure of the glycoprotein hexamer was resolved at 3.0-nm resolution as indicated by Fourier shell correlation at 0.143. For comparison to the structure of the RVFV hexameric capsomer, one capsomer was extracted from the published reconstruction (18) and filtered to 3-nm resolution.

RESULTS

Uukuniemi virus as a model system to study Phlebovirus fusion—We chose UUKV as a model system to study phlebovirus fusion to target membranes, because UUKV has been a preferred model system to study phlebovirus entry earlier (11, 12). Unlike RVFV and SFTSV, which require high biosafety containment levels, UUKV is apathogenic and can be handled safely at a lower biosafety containment level.

It is widely assumed that the G_C proteins of phleboviruses share the class II fusion protein fold. We confirmed this assumption by bioinformatics analysis using the protein homology/analogy recognition engine (Phyre²), which allows detecting structural homologs even in the absence of notable sequence similarity (32). UUKV G_C protein sequence (UniProt:P09613) matched the best with RVFV G_C (UniProt: P03518; 26% identity) and 86% of the modeled UUKV G_C structure (residues 1–428 of total 495) could be modeled against the known RVFV G_C structure (PDB:4HJ1) with 100% confidence. This strongly supports the notion that the two proteins are homologous and share the same class II fusion protein fold.

Electron cryo-tomography structure of native UUKV—We studied the pre-fusion conformation of native UUKV particles at pH 7.5 by electron cryomicroscopy and tomography. Two-dimensional micrographs and three-dimensional tomographic reconstructions revealed particles that were nearly spherical in shape (Fig. 1A,B). The particles displayed a

continuous layer of glycoprotein capsomers on the surface. Sub-tomogram averaging of ~3,000 glycoprotein capsomers from ~100 virions at pH 7.5 yielded a structure of the native hexameric capsomer (width ~17 nm, height ~10 nm) at 3.0 nm resolution (Fig. 1C–E; UUKV). This structure revealed a striking similarity to the cylindrically shaped hexameric capsomer of RVFV (18, 33) (Fig. 1C–E; RVFV), but was different from the structure of the UUKV glycoprotein capsomers at neutral pH, fixed with glutaraldehyde, that we have reported earlier (34). The latter had a more pointed and elongated morphology (height ~13 nm) and may correspond to a transient, extended conformation of the capsomers captured by the fixative. In conclusion, the native UUKV glycoproteins at pH 7.5 are organized as capsomers with a cylindrical shape comparable to that of the RVFV glycoprotein capsomers.

Fluorescent membrane labeling of UUKV—Enveloped virus glycoprotein catalyzed fusion to target membranes has been studied earlier in virus–liposome fusion assays exploiting fluorescent membrane labeling (35, 36). Lipid mixing between virus and liposomes can be monitored by measuring changes in fluorescence upon dilution of pyrene-labeled phospholipids from metabolically labeled virions to unlabelled liposomes following a pH drop, as first described for vesicular stomatitis virus (35). Before conducting such experiments with UUKV, we confirmed the incorporation of fluorescent pyrene in sufficient amounts in the viral membrane to form excited dimers (excimers). Pyrene excimers emit a red-shifted fluorescence in the visible spectrum, as compared to monomeric pyrene, which emits in the UV range. As expected, pyrene excimers emitted light at 475 nm when excited at 345 nm and could be diluted almost completely to monomers not emitting at 475 nm, by addition of detergent (Fig. 2A).

In general, UUKV preparations have a rather high (>500) particle-to-PFU ratio (12). However, both labeled and un-labeled viruses had similar infectivity, as estimated by titration assays of viral preparations, in combination with SDS-PAGE analysis. The specific infectivity of UUKV and UUKV-pyr was $3.0 \times 10^6 \pm 0.9 \times 10^6$ FFU/ μ g (N=2) and $7.4 \times 10^6 \pm 2.4 \times 10^6$ FFU/ μ g

(N=3), respectively (values are given as mean FFU per μ g of viral glycoprotein \pm standard error). This showed that pyrene is incorporated into the virus particles at significant levels and without adverse effects on virus infectivity.

Similarly to UUKV-pyr, and to what has been published before (36), we also produced pyrene-labeled SFV (SFV-pyr) to use it as a control in our assays. SFV-pyr behaved similarly to UUKV-pyr (Fig. 2B).

Late endosomal phospholipid bis(monoacylglycerol)phosphate (BMP) promotes lipid mixing—To study which target membrane phospholipid species have the potential to promote UUKV fusion, we used liposomes with different lipid compositions (Table 1). Because UUKV is believed to penetrate host cells from late endosomes (12) and may thus be expected to also undergo fusion in late endosomes, we hypothesized that not only late endosomal pH (below pH 6) but also the late endosomal lipid BMP may promote UUKV fusion. This lipid is highly abundant in the LE, constituting 15 mol% of the total LE phospholipids on the average and as high as 60 mol% in some LE fractions (37). Supporting our hypothesis, the presence of BMP promoted lipid mixing; at pH 5.0, UUKV-pyr could rapidly fuse to liposomes containing intermediate amounts of BMP (30 mol%; Fig. 3A). Most of the lipid mixing took place in the first few seconds after the pH drop (Fig. 3B) and reached maximal lipid mixing of 60% after 10 minutes (Fig. 3A).

To further validate this result, we compared the lipid requirements of UUKV-pyr to SFV-pyr, for which the conditions are well-characterized (22, 25, 38, 39). At pH 5.0, no lipid mixing was observed between UUKV-pyr and the liposomes containing cholesterol and/or sphingomyelin but lacking BMP (Fig. 3C). Conversely, and consistent with earlier observations (22, 25), efficient SFV-pyr lipid mixing only occurred with liposomes containing both cholesterol and sphingomyelin (Fig. 3C).

Unexpectedly, SFV-pyr also showed some lipid mixing to liposomes containing BMP in the absence of cholesterol and sphingomyelin (Fig. 3C). However, at pH 5.5, which is closer to the physiological SFV fusion threshold of pH ~6 (9), lipid mixing to these liposomes was at background level (Fig. 3D), whereas UUKV-pyr

still showed ~50% lipid mixing (see Fig. 6A).

BMP promotes UUKV-induced cell–cell fusion at the plasma membrane—Alternative to virus–liposome fusion assays, virus fusion can be studied by forcing the fusion at the plasma membrane. In such a ‘fusion-from-without’ assay, fusion events lead to syncytia formation, where two or more cells have fused together (40).

To further study the role of the anionic phospholipid BMP in UUKV fusion, we measured fusion of UUKV to BHK-21 cells, either in presence or absence of added BMP (Fig. 4A). We observed significantly increased levels of UUKV-induced cell–cell fusion at pH 5.0 when BMP was added to the cells before virus-binding and acidification/re-neutralization (Fig. 4B). However, if BMP was added after acidification/re-neutralization, fusion remained at basal level (Fig. 4B). When only BMP, but no virus, was added, no significant fusion could be observed (not shown). As a control, the assay was repeated with SFV, which does not require BMP (22, 25). No increase in fusion was observed; in fact in the presence of BMP, significantly ($P=0.002$) less fusion (0.25 ± 0.10) was observed than in its absence (0.33 ± 0.13).

Although the precise step at which BMP facilitates fusion remains unknown, these experiments further confirmed that BMP increases fusion between UUKV and target membranes. Interestingly, it has been demonstrated earlier in fusion-from-without assays that anionic lipids also promote fusion of dengue virus (20).

Viral glycoproteins are required for low pH mediated lipid mixing to BMP-containing liposomes—It has been previously reported that liposomes containing BMP can be intrinsically fusogenic at low pH (37). To exclude the possibility that the observed UUKV-pyr lipid mixing is passively caused by BMP in our assay, we produced pyrene-labeled donor liposomes (Lipo-pyr) containing similar monomer-to-excimer ratios than UUKV-pyr (Fig. 5A), and with practically the same phospholipid composition (Table 1) as reported for the UUKV virion earlier (41). We also included 25 mol% cholesterol in accordance with cholesterol levels found in the Golgi apparatus (42), the site of UUKV maturation (43). The fluorescent probe

in the donor liposomes was a pyrene labeled phospholipid analog 1-hexadecanoyl-2-(1-pyrenedecanoyl)-sn-glycero-3-phosphocholine (PC-pyr). Importantly, lipid mixing between pyrene-labelled donor liposomes and acceptor liposomes with BMP was at background level (Fig. 5B), showing that in our assay, glycoprotein-independent fusion played an insignificant role. Taken together, these results show that UUKV glycoproteins play an active role in promoting fusion to BMP-containing liposomes.

Lipid mixing requires late endosomal pH and physiological temperatures—The activation of the phlebovirus fusion machinery by acidic pH has been studied earlier by fusion-from-without assays. This has been demonstrated to occur at $\text{pH}<5.4$ for UUKV particles (12) and at $\text{pH}<5.7$ for RVFV (44) bound to the plasma membrane of BHK-21 cells. Consistent with this result, in our virus–liposomes fusion assay, we observed only minimal lipid mixing at neutral pH ($<10\%$), whereas 50% efficiency was reached at pH 5.6 and the maximal efficiency below pH 5.0 (Fig. 6A). These observations are compatible with UUKV entry from late endosomes.

Lipid mixing efficiency was temperature dependent. Lipid mixing decreased rapidly at temperatures below 37°C (Fig. 6B). For comparison, in an earlier UUKV fusion-from-without assay, fusion was reduced only by 30% at 20°C when compared to the situation at 37°C (12). The quantitative differences in the total extent of fusion, observed between our results with liposomes and the previously published results in presence of cells, was probably due to using two different experimental systems. We conclude that UUKV lipid mixing to liposomes shows steep temperature dependence.

UUKV-induced content release from BMP-containing liposome at low pH—The viral membrane fusion mechanism is thought to involve i. a conformational change in the viral fusion proteins that is triggered by low pH and that leads to the insertion of the fusion peptides into the target membrane, ii. further conformational changes bringing donor and acceptor membranes into close proximity, followed by mixing of the outer leaflets of the two membranes leading to hemifusion, iii.

progression from the hemi-fusion intermediate to fusion pore formation, leading to lipid mixing between the inner leaflets of the two membranes, and finally, iv. fusion pore expansion, leading to content mixing between the two fused compartments (45-47).

Because partial lipid mixing already occurs in the hemi-fusion state, lipid mixing alone is not indicative of full fusion. To this end, we sought to measure content release from content-labeled liposomes in presence of UUKV at low pH. We used liposomes that encapsulated a water-soluble fluorescent dye, sulforhodamine B (SRB), in self-quenching concentrations (48, 49). Leakage of SRB from the liposomes, either due to fusion pore opening and subsequent SRB release into the virus interior, or due to SRB leakage to the surrounding solution, leads to dilution of SRB. This in turn results in dequenching of fluorescence that can be measured (49). To allow measuring lipid mixing and content release in parallel, we used UUKV-pyr in these experiments.

Significant content release, as measured by SRB dequenching, occurred rapidly when UUKV was mixed with DOPC-DOPE-BMP-SRB liposomes (Fig. 7A,C) at 37°C and pH 5.0, but not with DOPC-DOPE-SRB liposomes (Fig. 7B,C). Some dequenching occurred over time also in the absence of the virus, suggesting that some dye leaked out from the acidified liposomes spontaneously (Fig. 7A,B). This is in contrast to earlier findings indicating that SRB-labeled DOPC liposomes were fully stable at pH 5.0 (49) and likely reflects the different lipid composition of the liposomes.

Content release was concomitant to lipid mixing, with no detectable delay (Fig. 7D). As the measured content release is a time average of several largely unsynchronized events, short delays in fusion pore opening cannot be detected with this assay. Single virus fusion assays are expected to yield more accurate information on the kinetics of hemi-fusion intermediate formation and fusion pore formation, as has been demonstrated for influenza virus earlier (50). Furthermore, we cannot exclude the possibility that some, if not all of the observed content release corresponds to ‘leaky fusion’, where soluble dye leaks out of the liposomes into the surrounding solution, instead of entering the

viral interior through a fusion pore. Taken together, these data show a clear virus-induced target membrane destabilization in presence of the phospholipid BMP, leading to liposome content release.

Anionic phospholipids with negative spontaneous curvatures promote fusion—What properties of BMP facilitate UUKV fusion? As the BMP headgroup is negatively charged, we hypothesized that negative charge is required for lipid mixing and thus also for full fusion. To test this hypothesis, we included liposomes containing three other phospholipids with negatively charged headgroups, namely DOPG, phosphatidic acid (PA) and DOPS, in our assays (Figure 8A). One should note that none of these lipids are usually enriched in the inner membrane leaflets of late endosomes and thus are not expected to be physiologically relevant for UUKV fusion. Similarly to BMP, DOPG and PA facilitated efficient lipid mixing at pH 5.0. However, contrary to our hypothesis, no significant lipid mixing was observed in presence of DOPS (Fig. 8B).

Which properties differentiate DOPS from the other anionic lipids tested? Unlike PA (51), PG (52), and BMP (37), which are thought to have negative spontaneous curvature at neutral pH, PS has been reported to have positive spontaneous curvature at neutral pH (53). Thus, negative spontaneous curvature might be one of the properties that promote UUKV lipid mixing. This hypothesis is in agreement with current membrane fusion models, which emphasize the role of phospholipids with negative spontaneous curvature in promoting lipid mixing (46, 54).

Interestingly, the spontaneous curvature of PS is known to change from positive to negative at pH 4.0 (53). Thus, if our hypothesis is correct and UUKV lipid mixing is promoted by both negative charge and negative curvature, also PS should promote fusion at pH 4.0. To test this, we measured UUKV lipid mixing at pH 4.0 to DOPC-DOPE-DOPS liposomes. In support of our hypothesis, significant lipid mixing (fusion index of 0.33 ± 0.03 , compared to 0.09 ± 0.02 with DOPC-DOPE liposomes; $P=0.0007$, $N=3$) was observed. In addition, as the zwitterionic DOPE that has negative spontaneous curvature did not promote UUKV lipid mixing (see Fig. 3C, Lipo), curvature may not be the only factor

promoting lipid mixing. Instead, our data suggests that both negative charge and negative spontaneous curvature are among the chemical and physical factors that promote UUKV fusion with lipid bilayers.

Electron cryo-tomography of the UUKV–liposome fusion complexes—Having found and characterized the minimal conditions for UUKV fusion with liposomes, we proceeded to study possible fusion intermediates by using electron cryo-tomography (Fig. 9). As expected, no UUKV–liposome fusion complexes were observed in the neutral pH control (Fig. 9A). However, UUKV mixed with BMP-containing liposomes at pH 5.0 revealed three different types of virus–liposome fusion complexes (Fig. 9B–D). First, clusters of viral glycoprotein capsomers in an elongated conformation (membrane-to-membrane distance ~18 nm) were observed to connect the viral membrane to the liposome membrane (Fig. 9B,C). These elongated capsomers match the length of the RVFV G_C protein in the observed extended conformation (14) (Fig. 9C, inset) and were clearly different from capsomers at neutral pH (Fig. 1A,B; Fig. 9A) and capsomers in other areas of the virion (Fig. 9B–D), which were ~10 nm in length. This conformation was also observed in acidified liposomes that lacked BMP (not shown) suggesting that BMP is not required for inducing this conformation. Second, and similarly to what has been observed in influenza virus (49), UUKV readily induced high curvature regions, or ‘dimples’, on the liposome membrane at liposome–virus contact sites (Fig. 9D, top). Third, we also observed a putative fusion site where the viral membrane was continuous with the liposome membrane (Fig. 9D, bottom). As these observations provide snapshots of the fusion process, we cannot exclude the possibility that some observed structures, for example capsomers in the elongated conformation, correspond to dead-end structures that would not culminate in fusion. Despite this limitation, our results provide direct evidence that UUKV undergoes fusion with BMP-containing membranes at pH 5.0. This is probably mediated by a conformational change in the viral glycoprotein capsomers taking place at virus membrane contact sites but further studies are required to verify this.

DISCUSSION

We established a minimal component virus–liposome model system for biophysical and structural characterization of phlebovirus fusion. Acidic pH was necessary but not sufficient for efficient UUKV fusion to liposomes; negatively charged phospholipids with a conical shape, notably BMP, were shown to facilitate efficient lipid mixing and content release.

Electron cryo-tomography and sub-tomogram averaging of UUKV glycoprotein capsomers revealed a structure similar to that of RVFV (17, 18). Furthermore, by using computational fold-recognition, we verified the assignment of UUKV G_C into the class II of viral fusion glycoproteins. These results suggest a high degree of structural conservation between the two phleboviral G_C glycoproteins.

It is widely accepted that acid-induced conformational changes in the class II viral fusion glycoprotein lead to the insertion of a hydrophobic fusion peptide in the target membrane via a transient extended conformation (47). Interestingly, electron cryo-tomography of UUKV–liposome mixtures acidified to pH 5.0 revealed elongated capsomer clusters bridging viral and liposome membranes. We attribute the appearance of these elongated capsomers to conformational changes in UUKV G_C fusion glycoprotein. These changes may correspond to either straightening of the G_C structure or to reorientation of G_C relative to the viral membrane. These elongated capsomers were limited to virus–target membrane contact sites. It is possible that in the parts of the virus that are not facing a target membrane, either no conformational changes take place, or the G_C glycoprotein folds back onto the virion surface to shield the hydrophobic fusion loop from the surrounding aqueous environment as much as possible. Similar elongated capsomer clusters have recently been observed in alphavirus–liposome complexes studied by electron cryo-microscopy (55), suggesting that the extended glycoprotein conformation is a general feature of class II fusion glycoproteins. It is tempting to speculate that the observed extended low pH conformation is analogous to the extended conformation observed in the crystallographic structure of the deglycosylated RVFV fusion

glycoprotein G_C ectodomain (14) but this requires experimental verification.

What is the physiological relevance of the observed phospholipid and low pH dependence for UUKV fusion *in vivo*? A growing body of evidence suggests that not only pH, but also compartment specific lipids and cholesterol concentration regulate endocytotic virus entry (20, 56, 57). The concentration of cholesterol and sphingomyelin decreases during the endocytic route, whereas the concentration of BMP drastically increases in the late endosomes (58, 59). Our findings are consistent with the known host cell penetration site of UUKV (*i.e.* late endosomes). As expected, cholesterol and sphingomyelin did not promote UUKV lipid mixing. On the other hand, BMP did promote efficient lipid mixing and also content release. Thus it is possible that BMP acts an entry co-factor, but this notion requires verification in further studies.

An interesting parallel is emerging between UUKV and dengue virus, an important late penetrating virus that also harbors a class II fusion glycoprotein. Similarly to UUKV, dengue has been reported to undergo fusion mainly in the late endosomes (60). In virus–liposome fusion assays, efficient lipid mixing has been shown to occur at pH 5.3 between dengue virus and either PC-PE-phosphatidylinositol(PI)-BMP or PC-PE-PI-BMP-cholesterol liposomes, but not liposomes containing PC, PE, sphingomyelin, and cholesterol. The requirement for anionic lipids has been suggested to explain fusion in the LE (20). However, we also observed some differences in UUKV lipid mixing behavior, as compared to dengue. Levels of UUKV lipid mixing showed a clear discrimination between the species of negatively charged lipids tested. For example, phosphatidylserine did not allow lipid mixing at pH 5.0. This was in contrast to dengue virus, where lipid mixing levels to liposomes were statistically the same at pH 5.3, independently of whether phosphatidylserine, BMP, or phosphatidylglycerol was tested (20).

In conclusion, our results show that the anionic phospholipid BMP promotes phlebovirus membrane fusion in a virus–liposome model system. Further cell culture based studies are required to assess the role of

BMP during viral endocytosis. Furthermore, our work demonstrates that the UUKV fusion glycoprotein actively mediates low pH induced membrane fusion by undergoing a conformational change from a flat pre-fusion conformation to an elongated conformation attacking the target membrane. As viral membrane fusion is one of the major steps that could be targeted by antivirals to block virus entry, it will be of major interest to extend this study to other phleboviruses, many of which are important human and animal pathogens.

ACKNOWLEDGEMENTS

We thank A. Siebert for electron microscopy support, K. Grünwald for helpful suggestions and T. Bowden for critically reading the manuscript. Oxford Particle Imaging Centre electron microscopy facility was founded by a Wellcome Trust JIF award (060208/Z/00/Z). This work was supported by the Wellcome Trust core award (090532/Z/09/Z), by the Wellcome Trust equipment grant (093305/Z/10/Z), by the Mary Goodger scholarship (to D.B.), by the Academy of Finland (130750 and 218080 to J.T.H.), and by the European Research Council (ERC) under the European Union’s Horizon 2020 research and innovation programme (649053 to J.T.H.).

CONFLICT OF INTEREST

The authors declare that they have no conflicts of interest with the contents of this article.

AUTHOR CONTRIBUTIONS

DB and JTH designed the study, performed the experiments, analyzed the results, and wrote the paper. SH performed cell–cell fusion assays. AC performed electron cryotomography of native Uukuniemi virus. All authors reviewed the results and approved the final version of the manuscript.

REFERENCES

1. Walter, C. T., and Barr, J. N. (2011) Recent advances in the molecular and cellular biology of bunyaviruses. *J. Gen. Virol.* **92**, 2467–2484
2. Elliott, R. M. (1990) Molecular biology of the Bunyaviridae. *J. Gen. Virol.* **71** (Pt 3), 501–522
3. Prins, M., and Goldbach, R. (1998) The emerging problem of tospovirus infection and nonconventional methods of control. *Trends Microbiol.* **6**, 31–35
4. Ergönül, O. (2006) Crimean-Congo haemorrhagic fever. *Lancet Infect Dis.* **6**, 203–214
5. Ikegami, T., and Makino, S. (2011) The pathogenesis of Rift Valley fever. *Viruses.* **3**, 493–519
6. Xu, B., Liu, L., Huang, X., Ma, H., Zhang, Y., Du, Y., Wang, P., Tang, X., Wang, H., Kang, K., Zhang, S., Zhao, G., Wu, W., Yang, Y., Chen, H., Mu, F., and Chen, W. (2011) Metagenomic analysis of fever, thrombocytopenia and leukopenia syndrome (FTLS) in Henan Province, China: discovery of a new bunyavirus. *PLoS Pathog.* **7**, e1002369
7. Yu, X.-J., Liang, M.-F., Zhang, S.-Y., Liu, Y., Li, J.-D., Sun, Y.-L., Zhang, L., Zhang, Q.-F., Popov, V. L., Li, C., Qu, J., Li, Q., Zhang, Y.-P., Hai, R., Wu, W., Wang, Q., Zhan, F.-X., Wang, X.-J., Kan, B., Wang, S.-W., Wan, K.-L., Jing, H.-Q., Lu, J.-X., Yin, W.-W., Zhou, H., Guan, X.-H., Liu, J.-F., Bi, Z.-Q., Liu, G.-H., Ren, J., Wang, H., Zhao, Z., Song, J.-D., He, J.-R., Wan, T., Zhang, J.-S., Fu, X.-P., Sun, L.-N., Dong, X.-P., Feng, Z.-J., Yang, W.-Z., Hong, T., Zhang, Y., Walker, D. H., Wang, Y., and Li, D.-X. (2011) Fever with thrombocytopenia associated with a novel bunyavirus in China. *N. Engl. J. Med.* **364**, 1523–1532
8. Garigliany, M.-M., Bayrou, C., Kleijnen, D., Cassart, D., Jolly, S., Linden, A., and Desmecht, D. (2012) Schmallerberg virus: A new Shamonda/Sathuperi-like virus on the rise in Europe. *Antiviral Res.* 10.1016/j.antiviral.2012.05.014
9. Helenius, A., Kartenbeck, J., Simons, K., and Fries, E. (1980) On the entry of Semliki forest virus into BHK-21 cells. *J. Cell Biol.* **84**, 404–420
10. Marsh, M., and Helenius, A. (1980) Adsorptive endocytosis of Semliki Forest virus. *J. Mol. Biol.* **142**, 439–454
11. Lozach, P.-Y., Kühbacher, A., Meier, R., Mancini, R., Bitto, D., Bouloy, M., and Helenius, A. (2011) DC-SIGN as a receptor for phleboviruses. *Cell Host Microbe.* **10**, 75–88
12. Lozach, P.-Y., Mancini, R., Bitto, D., Meier, R., Oestereich, L., Overby, A. K., Pettersson, R. F., and Helenius, A. (2010) Entry of bunyaviruses into mammalian cells. *Cell Host Microbe.* **7**, 488–499
13. Harmon, B., Schudel, B. R., Maar, D., Kozina, C., Ikegami, T., Tseng, C.-T. K., and Negrete, O. A. (2012) Rift Valley Fever Virus Strain MP-12 Enters Mammalian Host Cells via Caveola-Mediated Endocytosis. *J. Virol.* **86**, 12954–12970
14. Dessau, M., and Modis, Y. (2013) Crystal structure of glycoprotein C from Rift Valley fever virus. *Proc Natl Acad Sci USA.* **110**, 1696–1701
15. Lescar, J., Roussel, A., Wien, M. W., Navaza, J., Fuller, S. D., Wengler, G., Wengler, G., and Rey, F. A. (2001) The Fusion glycoprotein shell of Semliki Forest virus: an icosahedral assembly primed for fusogenic activation at endosomal pH. *Cell.* **105**, 137–148
16. Rey, F. A., Heinz, F. X., Mandl, C., Kunz, C., and Harrison, S. C. (1995) The envelope glycoprotein from tick-borne encephalitis virus at 2 Å resolution. *Nature.* **375**, 291–298
17. Freiberg, A. N., Sherman, M. B., Morais, M. C., Holbrook, M. R., and Watowich, S. J. (2008) Three-dimensional organization of Rift Valley fever virus revealed by cryoelectron tomography. *J. Virol.* **82**, 10341–10348
18. Huiskonen, J. T., Overby, A. K., Weber, F., and Grünewald, K. (2009) Electron cryo-microscopy and single-particle averaging of Rift Valley fever virus: evidence for

- GN-GC glycoprotein heterodimers. *J. Virol.* **83**, 3762–3769
19. Modis, Y., Ogata, S., Clements, D., and Harrison, S. C. (2003) A ligand-binding pocket in the dengue virus envelope glycoprotein. *P Natl Acad Sci Usa.* **100**, 6986–6991
 20. Zaitseva, E., Yang, S.-T., Melikov, K., Pourmal, S., and Chernomordik, L. V. (2010) Dengue virus ensures its fusion in late endosomes using compartment-specific lipids. *PLoS Pathog.* **6**, e1001131
 21. Gallala, H. D., and Sandhoff, K. (2011) Biologic al function of the cellular lipid BMP-BMP as a key activator for cholesterol sorting and membrane digestion. *Neurochem. Res.* **36**, 1594–1600
 22. Bron, R., Wahlberg, J. M., Garoff, H., and Wilschut, J. (1993) Membrane fusion of Semliki Forest virus in a model system: correlation between fusion kinetics and structural changes in the envelope glycoprotein. *EMBO J.* **12**, 693–701
 23. Corver, J., Ortiz, A., Allison, S. L., Schlich, J., Heinz, F. X., and Wilschut, J. (2000) Membrane fusion activity of tick-borne encephalitis virus and recombinant subviral particles in a liposomal model system. *Virology.* **269**, 37–46
 24. Smit, J. M., Bittman, R., and Wilschut, J. (1999) Low-pH-dependent fusion of Sindbis virus with receptor-free cholesterol- and sphingolipid-containing liposomes. *J. Virol.* **73**, 8476–8484
 25. Nieva, J. L., Bron, R., Corver, J., and Wilschut, J. (1994) Membrane fusion of Semliki Forest virus requires sphingolipids in the target membrane. *EMBO J.* **13**, 2797–2804
 26. Cyrklaff, M., Roos, N., Gross, H., and Dubochet, J. (2011) Particle-surface interaction in thin vitrified films for cryo-electron microscopy. *J Microsc.* **175**, 135–142
 27. Mastronarde, D. N. (2005) Automated electron microscope tomography using robust prediction of specimen movements. *J. Struct. Biol.* **152**, 36–51
 28. Kremer, J., Mastronarde, D., and McIntosh, J. (1996) Computer visualization of three-dimensional image data using IMOD. *J. Struct. Biol.* **116**, 71–76
 29. Huiskonen, J. T., Hepojoki, J., Laurinmäki, P., Vaheri, A., Lankinen, H., Butcher, S. J., and Grünewald, K. (2010) Electron cryotomography of Tula hantavirus suggests a unique assembly paradigm for enveloped viruses. *J. Virol.* **84**, 4889–4897
 30. Huiskonen, J. T., Parsy, M.-L., Li, S., Bitto, D., Renner, M., and Bowden, T. A. (2014) Averaging of Viral Envelope Glycoprotein Spikes from Electron Cryotomography Reconstructions using Jsubtomo. *J Vis Exp.* 10.3791/51714
 31. Bowden, T. A., Bitto, D., McLees, A., Yeromonahos, C., Elliott, R. M., and Huiskonen, J. T. (2013) Orthobunyavirus ultrastructure and the curious tripodal glycoprotein spike. *PLoS Pathog.* **9**, e1003374
 32. Kelley, L. A., and Sternberg, M. J. E. (2009) Protein structure prediction on the Web: a case study using the Phyre server. *Nat Protoc.* **4**, 363–371
 33. Sherman, M. B., Freiberg, A. N., Holbrook, M. R., and Watowich, S. J. (2009) Single-particle cryo-electron microscopy of Rift Valley fever virus. *Virology.* **387**, 11–15
 34. Overby, A. K., Pettersson, R. F., Grünewald, K., and Huiskonen, J. T. (2008) Insights into bunyavirus architecture from electron cryotomography of Uukuniemi virus. *Proc Natl Acad Sci USA.* **105**, 2375–2379
 35. Pal, R., Barenholz, Y., and Wagner, R. R. (1988) Pyrene phospholipid as a biological fluorescent probe for studying fusion of virus membrane with liposomes. *Biochemistry.* **27**, 30–36
 36. Wahlberg, J. M., Bron, R., Wilschut, J., and Garoff, H. (1992) Membrane fusion of Semliki Forest virus involves homotrimers of the fusion protein. *J. Virol.* **66**, 7309–7318
 37. Kobayashi, T., Beuchat, M.-H., Chevallier, J., Makino, A., Mayran, N., Escola, J.-M., Lebrand, C., Cosson, P., Kobayashi, T., and Gruenberg, J. (2002) Separation and characterization of late endosomal membrane domains. *J. Biol. Chem.* **277**, 32157–32164
 38. Corver, J., Moesby, L., Erukulla, R. K.,

- Reddy, K. C., Bittman, R., and Wilschut, J. (1995) Sphingolipid-dependent fusion of Semliki Forest virus with cholesterol-containing liposomes requires both the 3-hydroxyl group and the double bond of the sphingolipid backbone. *J. Virol.* **69**, 3220–3223
39. Waarts, B.-L., Smit, J. M., Aneke, O. J. C., McInerney, G. M., Liljeström, P., Bittman, R., and Wilschut, J. (2005) Reversible acid-induced inactivation of the membrane fusion protein of Semliki Forest virus. *J. Virol.* **79**, 7942–7948
40. Bratt, M. A., and Gallaher, W. R. (1969) Preliminary analysis of the requirements for fusion from within and fusion from without by Newcastle disease virus. *Proc Natl Acad Sci USA.* **64**, 536–543
41. Renkonen, O., Kääriäinen, L., Pettersson, R., and Oker-Blom, N. (1972) The phospholipid composition of Uukuniemi virus, a non-cubical tick-borne arbovirus. *Virology.* **50**, 899–901
42. van Meer, G., Voelker, D. R., and Feigenson, G. W. (2008) Membrane lipids: where they are and how they behave. *Nat. Rev. Mol. Cell Biol.* **9**, 112–124
43. Kuismanen, E., Hedman, K., Saraste, J., and Pettersson, R. F. (1982) Uukuniemi virus maturation: accumulation of virus particles and viral antigens in the Golgi complex. *Mol. Cell. Biol.* **2**, 1444–1458
44. de Boer, S. M., Kortekaas, J., Spel, L., Rottier, P. J. M., Moormann, R. J. M., and Bosch, B. J. (2012) Acid-activated structural reorganization of the Rift Valley fever virus Gc fusion protein. *J. Virol.* 10.1128/JVI.01973-12
45. Chernomordik, L. V., Frolov, V. A., Leikina, E., Bronk, P., and Zimmerberg, J. (1998) The pathway of membrane fusion catalyzed by influenza hemagglutinin: restriction of lipids, hemifusion, and lipidic fusion pore formation. *J Cell Biol.* **140**, 1369–1382
46. Chernomordik, L. V., and Kozlov, M. M. (2008) Mechanics of membrane fusion. *Nat Struct Mol Biol.* **15**, 675–683
47. Harrison, S. C. (2008) Viral membrane fusion. *Nat Struct Mol Biol.* **15**, 690–698
48. Kyoung, M., Srivastava, A., Zhang, Y., Diao, J., Vrljic, M., Grob, P., Nogales, E., Chu, S., and Brunger, A. T. (2011) In vitro system capable of differentiating fast Ca²⁺-triggered content mixing from lipid exchange for mechanistic studies of neurotransmitter release. *Proc Natl Acad Sci USA.* **108**, E304–13
49. Lee, K. K. (2010) Architecture of a nascent viral fusion pore. *EMBO J.* **29**, 1299–1311
50. Floyd, D. L., Ragains, J. R., Skehel, J. J., Harrison, S. C., and van Oijen, A. M. (2008) Single-particle kinetics of influenza virus membrane fusion. *Proc Natl Acad Sci USA.* **105**, 15382–15387
51. Kooijman, E. E., Chupin, V., Fuller, N. L., Kozlov, M. M., de Kruijff, B., Burger, K. N. J., and Rand, P. R. (2005) Spontaneous curvature of phosphatidic acid and lysophosphatidic acid. *Biochemistry.* **44**, 2097–2102
52. Alley, S. H., Ces, O., Barahona, M., and Templer, R. H. (2008) X-ray diffraction measurement of the monolayer spontaneous curvature of dioleoylphosphatidylglycerol. *Chem. Phys. Lipids.* **154**, 64–67
53. Fuller, N., Benatti, C. R., and Rand, R. P. (2003) Curvature and bending constants for phosphatidylserine-containing membranes. *Biophys. J.* **85**, 1667–1674
54. Chernomordik, L. V., and Kozlov, M. M. (2003) Protein-lipid interplay in fusion and fission of biological membranes. *Annu. Rev. Biochem.* **72**, 175–207
55. Cao, S., and Zhang, W. (2013) Characterization of an early-stage fusion intermediate of Sindbis virus using cryoelectron microscopy. *Proc Natl Acad Sci USA.* **110**, 13362–13367
56. Umashankar, M., Sánchez-San Martín, C., Liao, M., Reilly, B., Guo, A., Taylor, G., and Kielian, M. (2008) Differential cholesterol binding by class II fusion proteins determines membrane fusion properties. *J. Virol.* **82**, 9245–9253
57. Amini-Bavil-Olyaei, S., Choi, Y. J., Lee, J. H., Shi, M., Huang, I.-C., Farzan, M., and Jung, J. U. (2013) The Antiviral Effector IFITM3 Disrupts Intracellular Cholesterol Homeostasis to Block Viral Entry. *Cell Host Microbe.* **13**, 452–464

58. Kolter, T., and Sandhoff, K. (2010) Lysosomal degradation of membrane lipids. *FEBS Lett.* **584**, 1700–1712
59. Möbius, W., van Donselaar, E., Ohno-Iwashita, Y., Shimada, Y., Heijnen, H. F. G., Slot, J. W., and Geuze, H. J. (2003) Recycling compartments and the internal vesicles of multivesicular bodies harbor most of the cholesterol found in the endocytic pathway. *Traffic*. **4**, 222–231
60. van der Schaar, H. M., Rust, M. J., Chen, C., van der Ende-Metselaar, H., Wilschut, J., Zhuang, X., and Smit, J. M. (2008) Dissecting the cell entry pathway of dengue virus by single-particle tracking in living cells. *PLoS Pathog.* **4**, e1000244

FIGURE LEGENDS

Figure 1. Electron cryo-tomography and sub-tomogram averaging of UUKV virus. (A) A 2D projection image of Uukuniemi (UUKV) virions at pH 7.5 collected at $-6\ \mu\text{m}$ defocus at 0° tilt. Gold nanoparticles ($\sim 10\ \text{nm}$ in diameter) have been added as fiducial markers to align images in tomographic tilt series. Virions were $\sim 110\ \text{nm}$ in diameter and covered in glycoprotein capsomers. Smaller particles ($\sim 50\ \text{nm}$) with virion-like morphology were occasionally observed (arrowhead). (B) A 10-nm thick slice through a 3D tomographic reconstruction of UUKV virions at pH 7.5 collected at $-6\ \mu\text{m}$ defocus. Scale bar = $100\ \text{nm}$ for *A* and *B*. (C) A surface rendering of the viral glycoprotein capsomers is shown for UUKV (left) and Rift Valley fever virus (RVFV; right, EMDB-1550) solved using sub-tomogram averaging (this study, UUKV) and single particle icosahedral averaging (RVFV) (18). In both cases, one hexameric capsomer that is surrounded by six neighboring capsomers is shown. (D–E) Slices ($6\ \text{nm}$ thick) through the density maps are shown parallel (*D*) and orthogonal (*E*) to the viral membrane (*M*). Dimensions of the capsomers are indicated. Scale bar = $15\ \text{nm}$ for *C–E*.

Figure 2. Membrane labeling of UUKV and SFV with pyrene. (A–B) Fluorescence emission spectra (excitation at $345\ \text{nm}$) are shown for pyrene-labeled Uukuniemi virus (UUKV-pyr) and Semliki Forest virus (SFV-pyr). Spectra were measured before (black) and after (gray) solubilizing the membrane with 0.2% w/v Triton X-100 (TX-100). Addition of TX-100 results in the solubilization of the membrane, and thus further dissociation of dimeric pyrene excimers. This is seen as increased emission (up arrows) at 378 and $395\ \text{nm}$ corresponding to the pyrene monomers and as disappearance (down arrows) of the broad emission peak at $475\ \text{nm}$ corresponding to the pyrene dimers.

Figure 3. BMP promotes lipid mixing between UUKV and liposomes. (A–B) Pyrene-labeled Uukuniemi virus (UUKV-pyr) was mixed with either DOPC-DOPE (Lipo w/o BMP) or DOPC-DOPE-BMP (Lipo w BMP) liposomes and pre-incubated at 37°C . After acidification to pH 5, lipid mixing was followed over time. In the presence of BMP, efficient lipid mixing was observed and, after $600\ \text{s}$, a plateau was reached at lipid mixing index of ~ 0.6 . No significant lipid mixing was observed in the absence of BMP. The first $25\ \text{s}$ (indicated with a box in *A*) are shown in *B*. Most of the lipid mixing occurred in the first few seconds after acidification. (C) Quantification of UUKV-pyr and pyrene-labeled Semliki Forest virus (SFV-pyr; control) lipid mixing at 5 minutes post-acidification in presence of liposomes. In addition to control DOPC-DOPE liposomes (Lipo), liposomes with added lipids were tested as indicated. As expected, SFV lipid mixing required both sphingomyelin (SPM) and cholesterol (Chol), whereas UUKV lipid mixing was only observed in presence of BMP. (D) Quantification of SFV-pyr lipid mixing after 5 min at pH 5.5. No significant lipid mixing was observed in the presence of BMP and in the absence of SPM and Chol. Note that the Y-axis is on a different scale in *C* and *D*. Error bars represent one standard deviation ($N=3$). Statistical significance was determined using a Student's *t*-test using significance levels * $p \leq 0.05$, ** $p \leq 0.01$, *** $p \leq 0.001$.

Figure 4. BMP promotes UUKV-induced fusion of BHK-21 cells. (A) Uukuniemi virus (UUKV)-induced cell–cell fusion visualized by fluorescence confocal microscopy. UUKV was added to BHK-21 cells, cell–cell fusion was induced by acidification to pH 5.0, and cell nuclei (blue) and plasma membrane (orange) were stained for counting the number of syncytia (*i.e.* cells with multiple nuclei). As a negative control, cells were first imaged without added virus or BMP (1). In the absence of added BMP, and in the presence of UUKV, some syncytia could be observed (2). The effect of BMP on syncytia formation was tested by adding BMP either before (3) or after (4) acidification. Scale bar = $25\ \mu\text{m}$. (B) Quantification of cell–cell fusion. Labels 1–4 are as in *A*. Note that BMP significantly increased syncytia formation only when added before acidification. Error bars represent the standard error of the mean of the fusion index. Statistical significance was determined using a Student's *t*-test using significance levels * $p \leq 0.05$, ** $p \leq 0.01$, *** $p \leq 0.001$.

0.01, *** $p \leq 0.001$.

Figure 5. UUKV glycoproteins are required for lipid mixing. (A) Fluorescence emission spectrum of liposomes (Lipo-pyr) with a phospholipid composition similar to pyrene-labeled UUKV with and without added Triton X-100. (B) Quantification of lipid mixing between pyrene-labeled liposomes (Lipo-pyr) or Lipo-pyr with 2.5% w/v sucrose and unlabeled liposomes with BMP at 10 min post-acidification, pH 5.0. Pyrene-labeled Uukuniemi virus (UUKV-pyr) was added as a positive control for lipid mixing. No significant lipid mixing was observed in the case of labeled donor liposomes. Error bars represent one standard deviation (N=3). Statistical significance was determined using a Student's t-test using significance levels * $p \leq 0.05$, ** $p \leq 0.01$, *** $p \leq 0.001$.

Figure 6. UUKV lipid mixing with liposomes is pH and temperature sensitive. (A) Lipid mixing of pyrene-labeled Uukuniemi virus (UUKV-pyr) with BMP containing liposomes was determined between pH 4.0–7.5 at 37°C. For accurate pH measurements, pH was measured after acidification for each data point. Error bars represent one standard deviation for both the pH (horizontal bars) and lipid mixing index (vertical bars; N=3). A sigmoidal curve was fitted and the confidence of the fit is indicated with dotted lines (95% confidence level). Half-maximal lipid mixing was achieved at pH 5.6 (dashed lines). (B) Lipid mixing of UUKV-pyr with BMP-containing liposomes was determined at pH 5.0 at different temperatures. Error bars represent one standard deviation (N=4). Statistical significance was determined using a Student's t-test using significance levels * $p \leq 0.05$, ** $p \leq 0.01$, *** $p \leq 0.001$.

Figure 7. UUKV induces content release from liposomes in the presence of BMP. (A–B) Lipid mixing of pyrene-labeled Uukuniemi virus (UUKV-pyr) with DOPC-DOPE liposomes labeled with SRB (Lipo-SRB) was determined at pH 5.0, 37°C. In the presence of BMP, a rapid UUKV-induced content release was observed as shown in *A*. In the absence of BMP, content release remained at background levels as shown in *B*. Notice that also in the absence of UUKV (black trace) some spontaneous release of SRB was observed. (C) Quantification of content release at 600 s post-acidification confirmed that UUKV-induced content release was significantly higher in the presence of BMP than in its absence. Furthermore, UUKV-induced content release was significantly higher than the spontaneous release of SRB dye from the liposomes. Error bars represent one standard deviation (N=3 for Lipo-SRB and N=4 for Lipo-SRB with BMP). Statistical significance was determined using a Student's t-test using significance levels * $p \leq 0.05$, ** $p \leq 0.01$, *** $p \leq 0.001$. (D) Simultaneous measurement of content release (black trace) and lipid mixing (gray trace) in the presence of UUKV-pyr and BMP containing liposomes labeled with SRB showed that content release starts concomitantly to lipid mixing and follows roughly the same kinetics.

Figure 8. UUKV lipid mixing with liposomes containing non-physiological anionic lipids. (A) Pyrene-labeled Uukuniemi virus (UUKV-pyr) lipid mixing was measured with control DOPC-DOPE liposomes (Lipo) and with three other DOPC-DOPE liposomes containing additional phospholipids with negatively charged head groups, namely phosphatidylglycerol (PG), phosphatidylserine (PS), and phosphatidic acid (PA). After acidification to pH 5.0, lipid mixing was followed over time. In the presence of PA and PG, efficient lipid mixing was observed. In the presence of PS, lipid mixing was at background level. (B) Quantification of UUKV-pyr lipid mixing at 5 minutes post-acidification in presence of the same liposomes as in *A*. Liposomes with PG and PA showed significantly higher lipid mixing than the control liposomes (Lipo). Error bars represent one standard deviation (N=3). Statistical significance was determined using a Student's t-test using significance levels * $p \leq 0.05$, ** $p \leq 0.01$, *** $p \leq 0.001$.

Figure 9. Electron cryo-tomography of UUKV fusion. (A–B) Shown are 10-nm thick tomographic slices of UUKV (V) with liposomes (L) at either pH 7.5 (control) or pH 5.0. Liposomes shown contained BMP and liposomes in the lower panel in *B* had also added cholesterol (see Table 1). Tomograms have

been low-pass filtered to 6 nm^{-1} spatial frequency to emphasize the membranes and capsomers. Scale bar = 50 nm. (C) A close-up of the areas indicated in *B* are shown. Regions with extended capsomer structures (magenta) connecting the virus membrane (yellow) to the liposome membrane (cyan) are indicated with arrowheads in the panel on the left and colored in the panel on the right. For size comparison, five G_C monomers in an extended conformation (PDB:4HJC)(14) were placed side by side in different orientations around the long axis and filtered to the same spatial frequency (inset). Note that such extended structures were also observed in the absence of BMP. Scale bar = 15 nm. (D) A dimple structure at the virus–liposome contact site (upper panel) and a putative full fusion site where viral and liposome membranes have fully merged (bottom panel) are indicated with arrowheads. Scale bar = 50 nm.

TABLES

Table 1. Liposome preparations

Lipids	Molar ratio
DOPC : DOPE	7.0 : 3.0
DOPC : DOPE : BMP	5.0 : 2.0 : 3.0
DOPC : DOPE : SPM : Chol	2.2 : 2.2 : 2.2 : 3.3
DOPC : DOPE : SPM	5.6 : 2.2 : 2.2
DOPC : DOPE : Chol	4.8 : 1.9 : 3.3
DOPC : DOPE : DOPS	5.0 : 2.0 : 3.0
DOPC : DOPE : DOPG	5.0 : 2.0 : 3.0
DOPC : DOPE : α PA	5.0 : 2.0 : 3.0
DOPC : DOPE : BMP : Chol	3.6 : 1.4 : 3.0 : 2.0
DOPC : DOPE : BMP : SPM : DOPS : PC-pyr : Chol	2.8 : 1.7 : 0.4 : 1.1 : 1.1 : 0.4 : 2.5

FIGURES

Figure 1

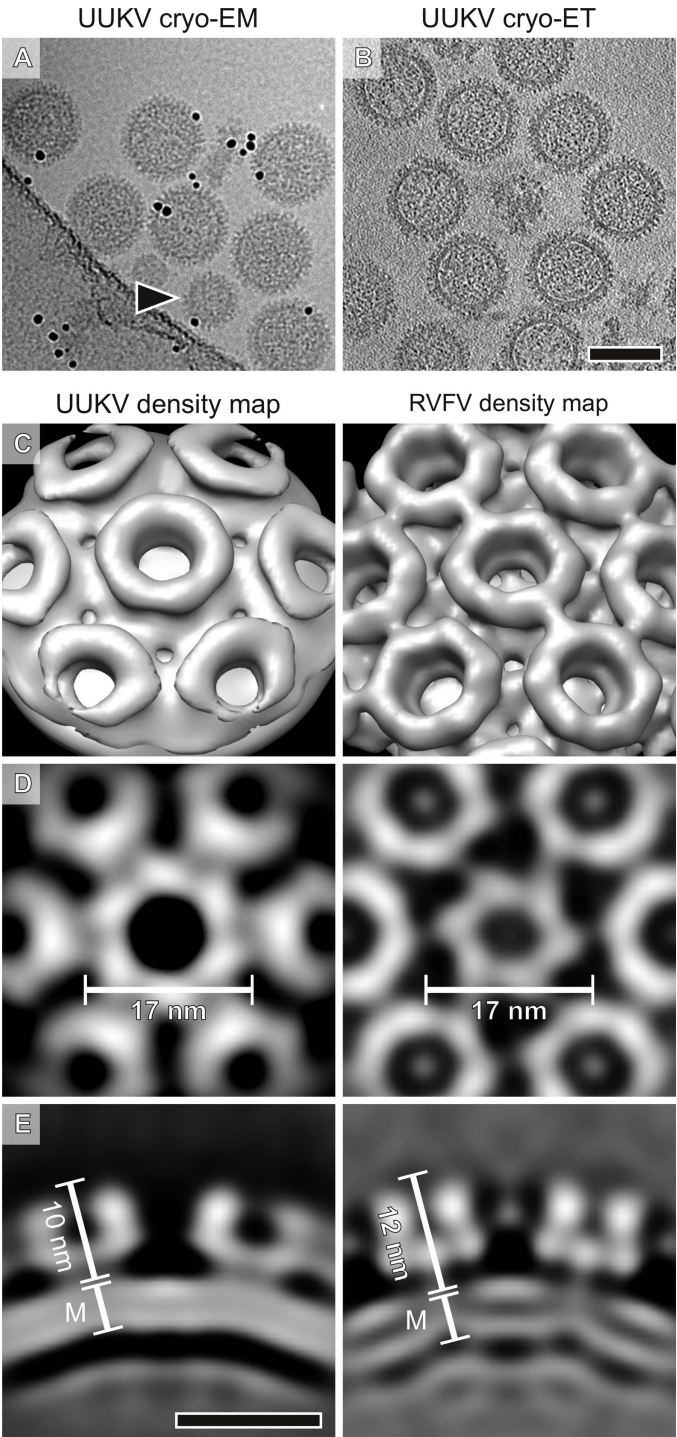


Figure 2

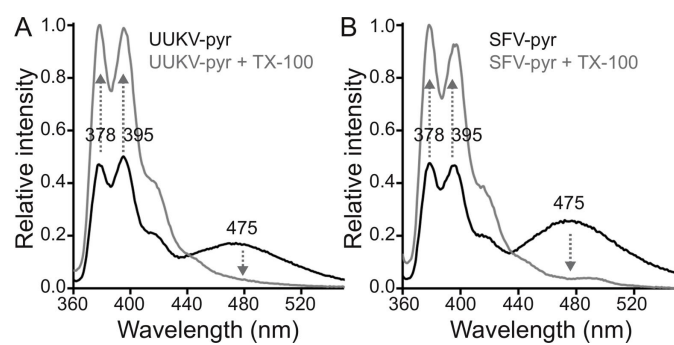


Figure 3

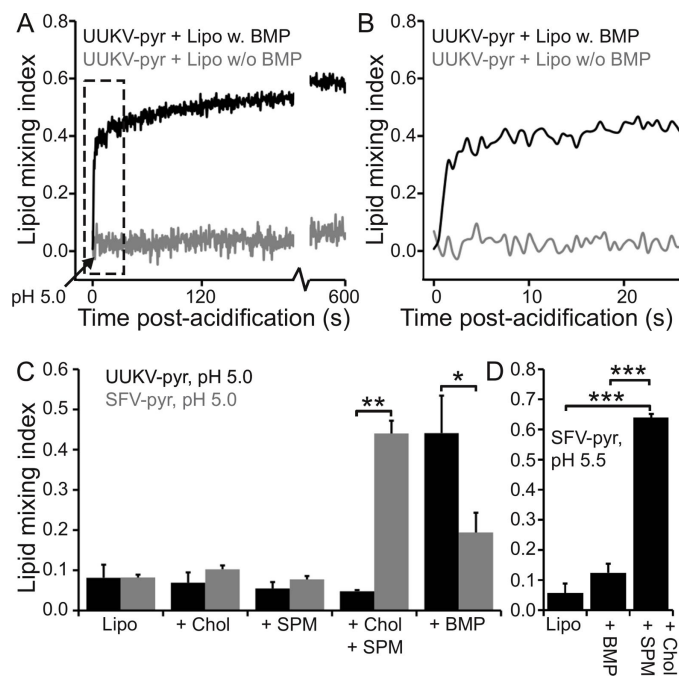


Figure 4

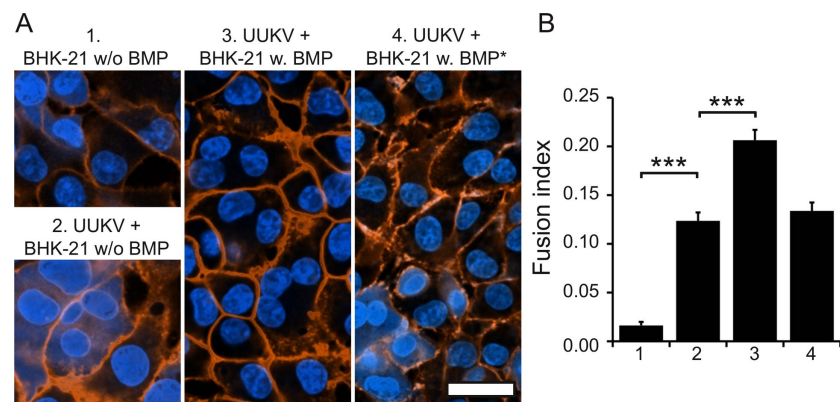


Figure 5

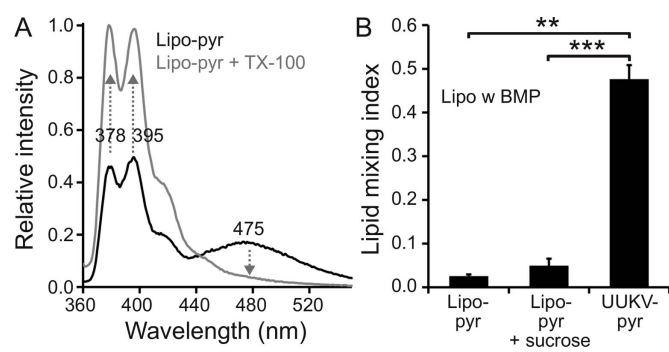


Figure 6

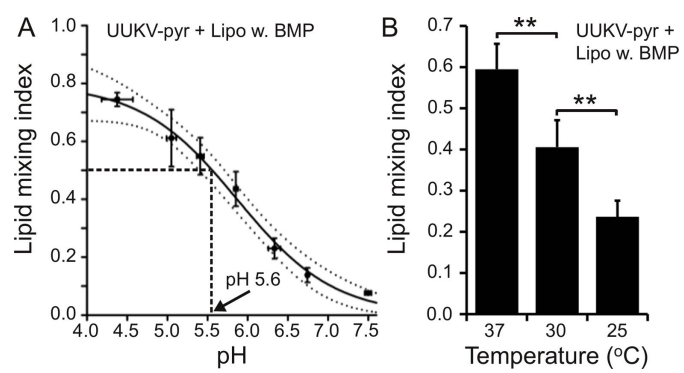


Figure 7

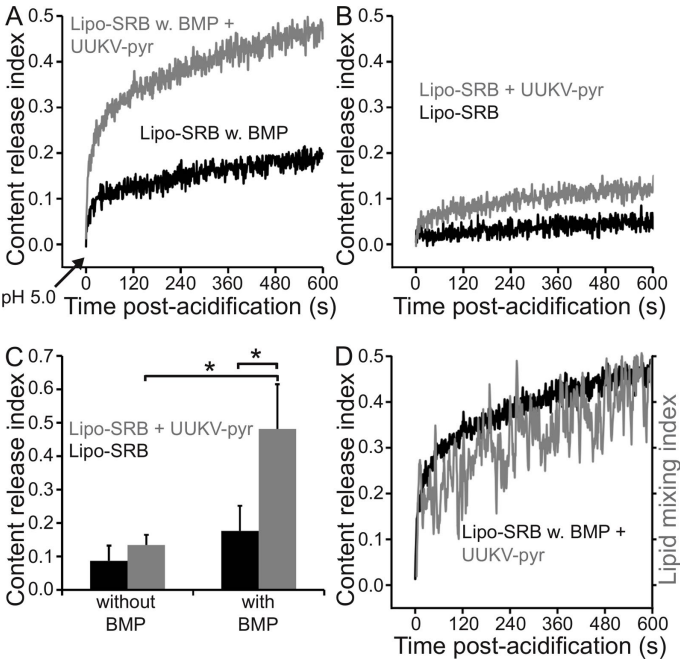


Figure 8

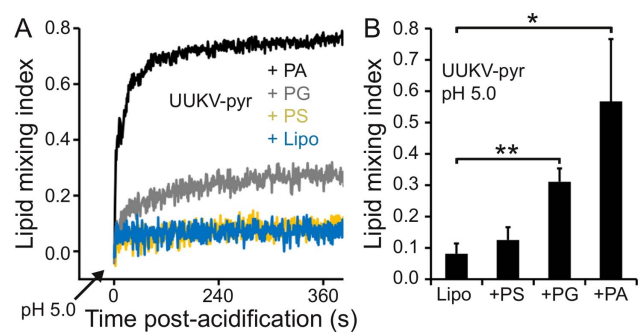


Figure 9

